

# A major asymmetric ice trap in a planet-forming disk:

## II. prominent SO and SO<sub>2</sub> pointing to C/O<1

Alice S. Booth<sup>1</sup>, Nienke van der Marel<sup>2,3</sup>, Margot Leemker<sup>1</sup>, Ewine F. van Dishoeck<sup>1,4</sup>, Satoshi Ohashi<sup>5</sup>

<sup>1</sup> Leiden Observatory, Leiden University, 2300 RA Leiden, the Netherlands  
e-mail: a booth@strw.leidenuniv.nl

<sup>2</sup> Physics & Astronomy Department, University of Victoria, 3800 Finnerty Road, Victoria, BC, V8P 5C2, Canada

<sup>3</sup> Banting Research fellow

<sup>4</sup> Max-Planck-Institut für Extraterrestrische Physik, Gießenbachstrasse 1, 85748 Garching, Germany

<sup>5</sup> RIKEN Cluster for Pioneering Research, 2-1, Hirosawa, Wako-shi, Saitama 351-0198, Japan

Received 12/04/2021; Accepted 7/06/2021

### ABSTRACT

Gas-phase sulphur bearing volatiles appear to be severely depleted in protoplanetary disks. The detection of CS and non-detections of SO and SO<sub>2</sub> in many disks have shown that the gas in the warm molecular layer, where giant planets accrete their atmospheres, has a high C/O ratio. In this letter, we report the detection of SO and SO<sub>2</sub> in the Oph-IRS 48 disk using ALMA. This is the first case of prominent SO<sub>2</sub> emission detected from a protoplanetary disk. The molecular emissions of both molecules is spatially correlated with the asymmetric dust trap. We propose that this is due to the sublimation of ices at the edge of the dust cavity and that the bulk of the ice reservoir is coincident with the millimeter dust grains. Depending on the partition of elemental sulphur between refractory and volatile materials the observed molecules can account for 15-100% of the total volatile sulphur budget in the disk. In strong contrast to previous results, we constrain the C/O ratio from the CS/SO ratio to be < 1 and potentially solar. This has important implications for the elemental composition of planets forming within the cavities of warm transition disks.

### 1. Introduction

New planetary systems are made from dust and gas in the rotating disks around young stars. Elemental abundances and ratios such as C/O are key quantities in linking planet composition to their formation history (Öberg et al. 2011; Booth et al. 2017; Eistrup et al. 2018). Sulphur is a particularly interesting element for astrophysics, vulcanology on young planets, and formation of life but its main reservoirs remain a puzzle. The depletion of elemental sulphur by 1-3 orders of magnitude in regions of dense gas has been an outstanding problem in astrochemistry for decades (e.g. Tieftrunk et al. 1994; Dutrey et al. 1997; Jenkins 2009). The bulk of the sulphur is thought to reside in refractory materials but the exact reservoir is still unconfirmed (Keller et al. 2002; Woods et al. 2015). In dark clouds and young (<1 Myr) Class 0/I sources sulphur-bearing molecules are routinely detected in the gas-phase but their contribution to the total sulphur budget and chemical origin are still somewhat unclear (e.g. Artur de la Villarmois et al. 2019; Le Gal et al. 2020; Garufi et al. 2021). On the ices, less is known aside from the direct detections of SO<sub>2</sub> and OCS, and an upper-limit for H<sub>2</sub>S, contributing to ≈5% of the total sulphur budget in protostars (Boogert et al. 1997, 2015). Indirectly, the ice composition can be inferred from observations of environments where ices sublimate, e.g., hot cores, and the gas detected in these systems suggests the presence of SO and SO<sub>2</sub> ices (Drozdovskaya et al. 2018; Tyshoniec et al. 2021).

In protoplanetary disks, a study of the elemental composition of the accreted disk material in the photopsheres of Herbig Ae/Be stars shows that ≈89±8% of the sulphur in disks is refractory (Kama et al. 2019). Therefore, the quest has been ongoing to detect different molecules to try and account for the total volatile fraction of sulphur in >1 Myr protoplanetary disks especially as

this is where gas-giant planets accrete the bulk of their atmospheres. Sulphur species may form of hazes in the atmosphere (He et al. 2020) and they are important for pre-biotic chemistry (Ranjan et al. 2018). CS is most commonly detected followed by H<sub>2</sub>CS (Le Gal et al. 2019; Codella et al. 2020; Fedele & Favre 2020), yet although CS is the most abundant sulphur species in protoplanetary disks, it only accounts for <1% of the total sulphur budget. There are only a few sources with detections of SO including the two Herbig disks, AB Aur and HD 100546 (Guilloteau et al. 2016; Fuente et al. 2010; Booth et al. 2018). There are one tentative detection of SO<sub>2</sub> (Semenov et al. 2018) and one detection of H<sub>2</sub>S (Phuong et al. 2018).

Even-though only a small fraction of volatile sulphur has been detected in disks so far, sulphur-species have provided key insight into the elemental make up of disk's atmospheres. The CS/SO ratio has been proposed as a tracer of the underlying C/O ratio in the gas. Detections of CS and non-detections/tentative detections of SO and SO<sub>2</sub> in many disks (LkCa 15, DM Tau, GO Tau, MWC 480 and PDS 70) indicate a high gas phase C/O ratio around unity in the warm molecular layer (Dutrey et al. 2011; Semenov et al. 2018; Facchini et al. 2021). These observations are directly probing where gas giant planets accrete their atmospheres (Morbidelli et al. 2014; Teague et al. 2019; Cridland et al. 2020). This high ratio is in line with the depletion of volatile C and O in disks that can be explained by the vertical mixing, radial transport, freeze-out and subsequent chemical re-processing of CO (e.g. Krijt et al. 2020), where more O than C is locked up in the ices. Observing sulphur-species is therefore an extremely useful and complementary tool in constraining the bulk elemental composition of the gas in disks.

Here we present the first measurements of SO and SO<sub>2</sub> in a disk that can be directly linked to an ice trap. Oph-IRS 48 is

a 2.0  $M_{\odot}$  Herbig A0 source located at 134 pc in the  $\rho$  Ophiuchus star forming region (Brown et al. 2012; Gaia Collaboration et al. 2018). This protostar is host to a transition disk with an extreme azimuthal asymmetry traced in the millimeter to cm sized grains (van der Marel et al. 2013, 2015) whereas the micron sized grains are distributed axisymmetrically (Geers et al. 2007). The dust cavity extends out to 60 au and the gas cavity traced in CO to 25 au with a depletion of gas in the cavity of  $\times 10^3$  relative to the ring (van der Marel et al. 2016). The disk is gas rich and warm with detections of the rarer CO isotopologues  $C^{18}O$  and  $C^{17}O$ , and  $H_2CO$  (Bruderer et al. 2014; van der Marel et al. 2014, 2016). The bulk of the gas, traced in CO, is present through-out the entire azimuth of disk, like the micron-sized grains, whereas the  $H_2CO$  was tentatively found to be co-spatial with the dust trap. This source presents a unique opportunity to study the chemistry associated with an exposed inner cavity edge and a high concentration of large icy dust grains. In van der Marel & et al. (2021), hereafter Paper I, we present new detections of  $H_2CO$  and  $CH_3OH$  in the Oph-IRS 48 protoplanetary disk and here in Paper II we present observations of the S-bearing molecules:  $SO_2$ ,  $^{34}SO_2$ , SO and CS. In Section 2 we outline these observations and in Section 3 we show the resulting images and inferred column densities. In Section 4 we discuss the total volatile sulphur detected in the disk compared to the total Sulphur budget, investigate the chemical origin of the detected species and the link to the dust trap, and provide key constraints on the C/O of the gas that differ from other disks observed so far.

## 2. Observations

We utilise two sets of Band 7 observations of Oph-IRS 48 taken with the Atacama Large Millimeter/submillimeter Array (ALMA) during Cycles 2 and 5. The Cycle 2 program 2013.1.00100.S (PI: Nienke van der Marel) were taken June and August 2015 and were calibrated using the provided calibration scripts. These data cover one transition of  $C^{18}O$ , SO and CS (see Table 1) and have native channel width of 122 kHz or  $\approx 0.23$  km s $^{-1}$  and a spatial resolution of  $\approx 0''.2$ . The Cycle 5 program 2017.1.00834.S (PI: Adriana Pohl) was taken in August 2018. For full details on the data calibration see Ohashi et al. (2020) where the continuum polarization data are presented. This paper focuses on the detection of two  $SO_2$  lines and one  $^{34}SO_2$  line (see Table 1) in these data. The detected  $H_2CO$  and  $CH_3OH$  lines are the focus of Paper I. These line data all have a channel width of 1953 kHz or  $\approx 1.7$  km s $^{-1}$  and a spatial resolution of  $\approx 0''.5$ .

We use the continuum images from both 2013.1.00100.S and Ohashi et al. (2020), and the higher spatial resolution Francis & van der Marel (2020) image to compare to the respective line images. All of the lines were imaged using CASA `tcLEAN` with robust weighting of 0.5 and a Keplerian mask (with an inclination angle of  $50^\circ$  and position angle of  $100^\circ$ , van der Marel et al. e.g. 2021) and stellar mass of 2.0  $M_{\odot}$  and distance of 134 pc. Using the phase-centre variable in `tcLEAN` the central position is set to ICRS 16h27m37.1797s,  $-24^\circ 30' 35.480''$  computed using the Gaia DR2 position at the time of the observations (Gaia Collaboration et al. 2018) for the Cycle 5 data.

The resulting beam sizes, peak emission and per channel rms are listed in Table 1. All lines but the CS  $J = 7 - 6$  line are robustly detected ( $> 3\sigma$  emission over 3 consecutive channels) and the channel maps for the detected lines are shown in Appendix A.1. For the CS a  $3\sigma$  upper limit on the disk integrated

flux (see Table 1) was propagated from the rms noise in the channel maps following the method in Carney et al. (2019). To reduce the per channel rms and thus increase the signal-to-noise the Cycle 2  $SO\ 1_2 - 0_1$  line was imaged at 1.7 km s $^{-1}$ . This also matches the spectral resolution of the Cycle 5  $SO_2$  isotopologue lines.

## 3. Analysis

The Keplerian-masked integrated intensity maps for the  $C^{18}O$ ,  $SO_2$ ,  $^{34}SO_2$  and SO lines are presented in Figure 1 alongside the  $\approx 0''.2$  0.9 mm continuum.  $SO_2$  is clearly detected and this is the first prominent detection of this molecule in a protoplanetary disk. The  $SO_2$ ,  $^{34}SO_2$  and SO maps all show central dips in emission and are all highly asymmetric peaking in a similar azimuthal region of the disk as the mm-dust, much like the  $H_2CO$  and  $CH_3OH$  (see Paper I). This is in contrast to the  $C^{18}O$  which does also show a central cavity but is present throughout the full azimuth of the disk. To further investigate the spatial relationship between the dust and sulphur-bearing molecules radial and azimuthal profiles of both were generated. The radial profiles for the dust and molecular lines were averaged over a wedge from  $100^\circ$  to  $260^\circ$  relative to the north minor axis and are shown Appendix Fig A.2. The errors are given by the standard deviation of the intensity of the pixels ( $0''.1$  or  $0''.05$  for the SO) in each radial bin  $0''.2$  for the  $SO_2$  and  $^{34}SO_2$  and  $0''.1$  for the SO) divided by the square root of the number of beams per arc of the wedge. This highlights the spread in intensity values per bin rather than the intrinsic errors in the data themselves. In the lower resolution data the  $SO_2$  and  $^{34}SO_2$  lines peak just outside the dust radial peak but the higher resolution SO line is peaking at the same radial distance the dust emission.

The azimuthal profiles were extracted from an ellipse with the same position and inclination angle of the disk. For the  $SO_2$  and  $^{34}SO_2$  a de-projected radius of  $\approx 70$  au was chosen and for SO a radius of  $\approx 90$  au. The errors here are computed from the rms in the integrated intensity maps generated without a Keplerian mask. For comparison the normalised azimuthal profile of the 0.9 mm dust from the respective observations is shown. The  $SO_2$  lines have a slightly wider azimuthal extent than the dust and the optically thinner lines have slight dips where the dust emission peaks, potentially indicating continuum absorption of the line emission. This may indicate that for the  $SO_2$  the  $5_{3,3} - 4_{2,2}$  line ( $E_{up}$  of 36 K) is optically thick higher above the dust  $\tau = 1$  surface whereas the  $14_{4,10} - 14_{3,11}$  line ( $E_{up}$  of 136 K) is coming from a deeper region of the disk along the observing line of sight. In the Appendix in Fig A.3 we also show a comparison of the azimuthal profiles for the  $SO_2$  with the  $H_2CO$ ,  $CH_3OH$  from Paper I and the 0.9 mm dust. Here the  $H_2CO$  and  $SO_2$  are seen to have the same azimuthal extent but the  $CH_3OH$  is more compact and following the dust, similar to the higher resolution SO observations.

The total disk integrated line flux was extracted from the channel maps using a Keplerian mask and is listed in Table 1 with a 10% ALMA flux calibration error. These spectra are included in Appendix Fig A.2. There is no evidence for an additional component of emission or broader line-profiles than expected from a disk, as seen in HD 100546 in SO (Booth et al. 2018).

We calculate the average column densities of  $SO_2$ ,  $^{34}SO_2$  and SO (and an upper-limit on the CS column density) from the disk integrated fluxes. For this we assume the line emitting area to be the same as the  $5\sigma$  extent of the 0.9 mm dust emission

**Table 1.** Properties of the molecular lines and images analysed in this work.

Molecule	Transition	Frequency (GHz)	$\log_{10}(A_{ij})$ (s <sup>-1</sup> )	$E_{up}$ (K)	$g_u$	Beam	$\Delta v$ kms <sup>-1</sup>	Peak (mJy beam <sup>-1</sup> )	rms* (mJy beam <sup>-1</sup> )	Disk Int. Flux (mJy km s <sup>-1</sup> )
C <sup>18</sup> O	3 - 2	329.3305525	-5.6631	31.6	7	0'':20×0'':16 (65°)	0.23	58.45	5.10	896.5 ± 90
SO <sub>2</sub>	5 <sub>3,3</sub> - 4 <sub>2,2</sub>	351.2572233	-3.0672	35.9	11	0'':55×0'':44 (80°)	1.7	34.33	0.91	305.1 ± 31
SO <sub>2</sub>	14 <sub>4,10</sub> - 14 <sub>3,11</sub>	351.8738732	-3.4644	135.9	29	0'':55×0'':44 (80°)	1.7	13.87	0.91	124.9 ± 12
<sup>34</sup> SO <sub>2</sub>	6 <sub>3,3</sub> - 5 <sub>2,4</sub>	362.1582327	-3.4839	40.7	13	0'':53×0'':42 (80°)	1.7	12.11	1.20	87.3 ± 9
SO	1 <sub>2</sub> - 0 <sub>1</sub>	329.3854770	-4.8467	15.8	3	0'':20×0'':16 (65°)	1.7**	13.62	2.49	166.9 ± 17
CS	7-6	342.8828503	-3.0774	65.8	15	0'':20×0'':16 (65°)	0.23	-	8.23	<348 ± 35

\* per channel

\*\* Note the native channel width of these data is 0.23 km s<sup>-1</sup>.The values for the line frequencies, Einstein A coefficients, and upper energy levels ( $E_{up}$ ) and degeneracies ( $g_u$ ) are taken from the Cologne Database for Molecular Spectroscopy (CDMS) (Müller et al. 2005).

from Francis & van der Marel (2020) (see Figure A.4 in the Appendix). This is the same approach as in Paper I and is an area of  $1.2 \times 10^{-11}$  steradians. Following the method outlined in Goldsmith & Langer (1999) and applied to disks (e.g. Loomis et al. 2018) we construct an opacity-corrected rotational diagram for the SO<sub>2</sub> resulting in a rotational temperature of  $\approx 100$  K. This framework assumes LTE and that the lines are optically thin to marginally optically thick. We also calculate column densities for <sup>34</sup>SO<sub>2</sub>, SO and CS assuming an excitation temperature of 50, 100 and 150 K. The latter two are approximately the rotational temperatures derived for CH<sub>3</sub>OH and H<sub>2</sub>CO respectively in Paper I. The resulting values are listed in Table 2. The inferred SO<sub>2</sub>/<sup>32</sup>SO<sub>2</sub> is only 2 compared to the value of 22 for the <sup>32</sup>S/<sup>34</sup>S isotope ratio (e.g. Wilson 1999). This shows that the emission from the primary isotopologue, SO<sub>2</sub>, is optically thick. We therefore do not use the SO<sub>2</sub> column density derived from the SO<sub>2</sub> but rather using the rarer isotopologue <sup>34</sup>SO<sub>2</sub>. The ratio of CS/SO is <0.01 and CS/SO<sub>2</sub> <0.02 (using SO<sub>2</sub> derived from the <sup>34</sup>SO<sub>2</sub>). We note that as the inferred column densities are inversely proportional to the assumed emitting area our results may be a conservative lower limit.

As a complementary check for optically thick SO<sub>2</sub> we also calculate the brightness temperature of the 5<sub>3,3</sub>-4<sub>2,2</sub> line. This was done by re-imaging the line before continuum subtraction, calculating the peak intensity map (moment 8) and then converting this to a brightness temperature under the Rayleigh-Jeans approximation. We find that this results a low temperature with a peak of  $\approx 7$  K. This is most likely due to beam dilution as the emission is currently unresolved. A brightness temperature of  $\approx 100$  K would require an emitting area  $\approx 15\times$  smaller than the 0'':55×0'':44 beam of these data. Future 0'':1 data will be able to test this.

## 4. Discussion

### 4.1. Volatile sulphur in the IRS 48 disk

The bulk of the elemental sulphur in protoplanetary disks is thought to be in refractory materials ( $\approx 89 \pm 8\%$ ) (Kama et al. 2019). Therefore, it is interesting to calculate what fraction of the expected volatile sulphur abundance in the IRS 48 disk can be accounted for by the SO and SO<sub>2</sub> we detect. To estimate this we take the total volatile sulphur to be the sum of the SO<sub>2</sub> (from the <sup>34</sup>SO<sub>2</sub>) and SO average column densities. The  $N_H$  column density at 60 au from the IRS 48 disk model is  $1.6 \times 10^{22}$  cm<sup>-2</sup> where the gas density structure is constrained from C<sup>18</sup>O observations (Bruderer et al. 2014; van der Marel et al. 2016). This results in a S/H ratio of  $4.6\text{--}10.0 \times 10^{-7}$  (depending on the excitation temperature, see Table 2) which is  $\approx 15\text{--}100\%$  of the total

**Table 2.** Derived column densities and ratios

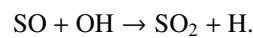
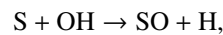
Molecule	$T_{ex}$ (K)	$N_T$ (cm <sup>-2</sup> )	$\tau$
SO <sub>2</sub> *	50	$2.6 \pm 0.3 \times 10^{15}$	[> 1]
	100	$4.4 \pm 0.4 \times 10^{15}$	[> 1]
	150	$6.6 \pm 0.4 \times 10^{15}$	[> 1]
<sup>34</sup> SO <sub>2</sub>	50	$1.2 \pm 0.1 \times 10^{14}$	[0.26]
	100	$2.0 \pm 0.2 \times 10^{14}$	[0.08]
	150	$3.0 \pm 0.3 \times 10^{14}$	[0.04]
SO	50	$4.7 \pm 0.5 \times 10^{15}$	[0.60]
	100	$7.1 \pm 0.7 \times 10^{15}$	[0.16]
	150	$9.9 \pm 1.0 \times 10^{15}$	[0.08]
CS	50	$\leq 5.9 \pm 0.6 \times 10^{13}$	[ $\leq 2.3$ ]
	100	$\leq 2.9 \pm 0.3 \times 10^{13}$	[ $\leq 0.35$ ]
	150	$\leq 3.2 \pm 0.3 \times 10^{13}$	[ $\leq 0.14$ ]
S/H	50	$4.6 \times 10^{-7}$	-
	100	$7.2 \times 10^{-7}$	-
	150	$1.0 \times 10^{-6}$	-
CS/SO	50	$\leq 0.012$	-
	100	$\leq 0.004$	-
	150	$\leq 0.003$	-
SO/SO <sub>2</sub>	50	1.8	-
	100	1.6	-
	150	1.5	-

\* using <sup>34</sup>SO<sub>2</sub> and <sup>32</sup>S/<sup>34</sup>S = 22

range in volatile S budget estimated by Kama et al. (2019). Although we can account for the bulk of the volatile sulphur in the disk with just the SO and SO<sub>2</sub> molecules, further observations targeting H<sub>2</sub>S and both oxygen and carbon bearing sulphur molecules (H<sub>2</sub>CS, CH<sub>3</sub>SH, OCS and C<sub>2</sub>S) will provide the complete picture as to how the volatile sulphur is partitioned in this disk.

### 4.2. Chemical origin of the SO and SO<sub>2</sub> in the IRS 48 disk

We find that SO and SO<sub>2</sub> gas in the IRS 48 disk is co-spatial with the asymmetric dust trap. If the SO and SO<sub>2</sub> are forming in the gas phase then the key reactions are (e.g. Charnley 1997):



Therefore gas phase formation of SO and SO<sub>2</sub> requires sufficient OH in the disk atmosphere. Interestingly *Herschel*/PACS reported non-detections of both OH and H<sub>2</sub>O in the IRS-48 disk (Fedele et al. 2013). Additionally as the molecules are co-spatial

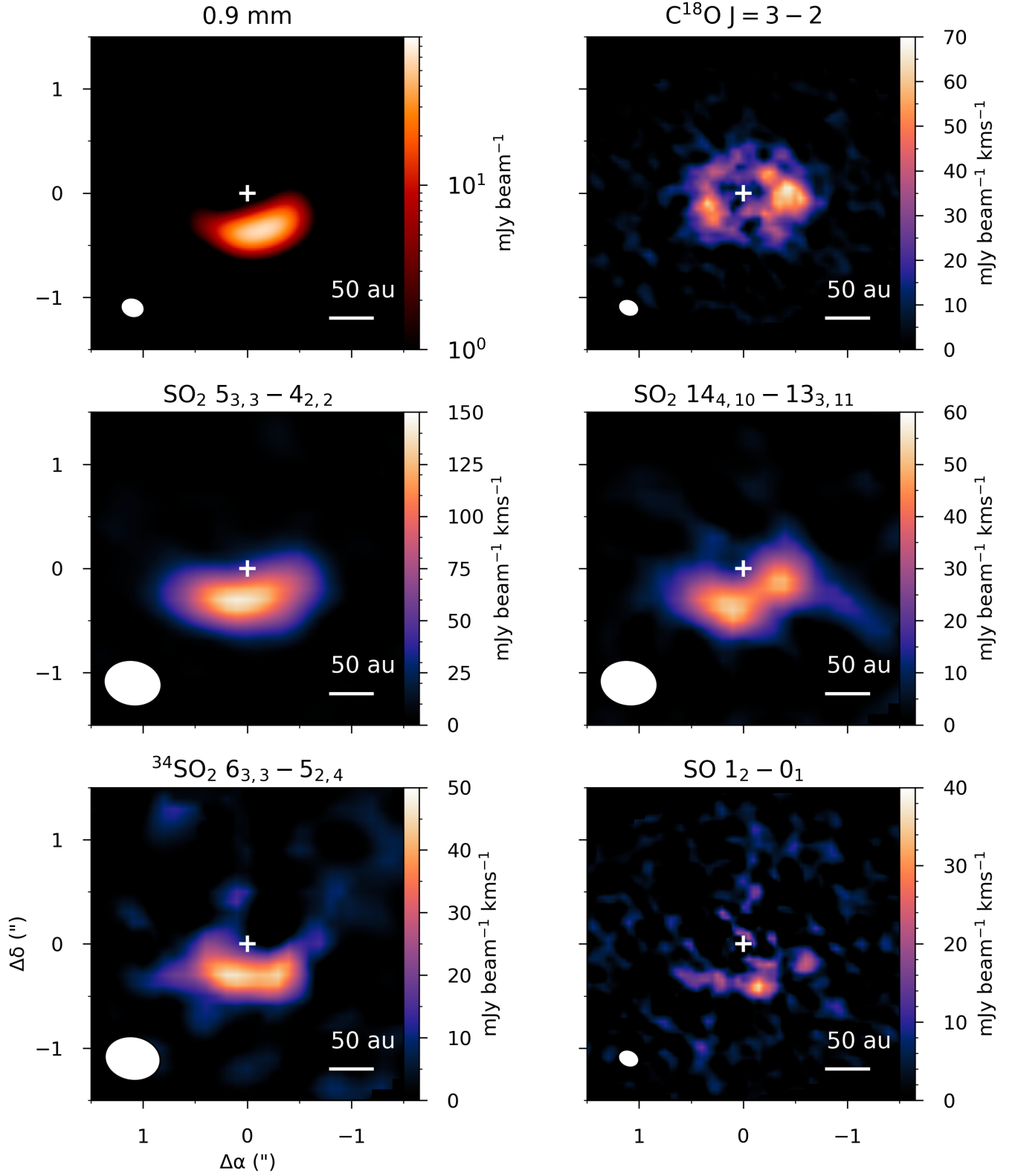


**Fig. 1.** Integrated intensity maps of the 0.9 mm continuum emission and detected lines listed in Table 1. The line maps are made with a Keplerian mask and the synthesised beam is shown in the bottom left corner of each panel.

with the dust trap this indicates that gas-grain processes are im- portant to consider too. The alternative origin for the gas-phase

SO and SO<sub>2</sub> that we propose is from the sublimation of ices, particular at the dust cavity wall (Cleeves et al. 2011; Booth et al. 2021). If the ice reservoir is constrained to the larger millimeter and cm-sized dust grains, as suggested for TW Hya (Salinas et al. 2016; Walsh et al. 2016), then this would explain the morphology of the molecular emission we see towards IRS 48. This could be either from the direct sublimation of SO and SO<sub>2</sub> ice or via gas-phase chemistry following the UV photo-dissociation of evaporated H<sub>2</sub>S and H<sub>2</sub>O ices. The sublimation temperatures of SO<sub>2</sub> and H<sub>2</sub>CO are similar so the azimuthal correlation of these species makes sense, and it follows that the CH<sub>3</sub>OH is more compact. As the SO data are of much higher spatial resolution and lower signal-to-noise a direct comparison to the other line spatial morphologies is not too meaningful.

The vortex in the IRS 48 disk may also play a role in the chemistry. Vertical convection cells in the vortex might also transport icy material from the disk midplane up into the warm molecular layer resulting in an increase in the sublimation of ices (Meheut et al. 2010) as suggested also for H<sub>2</sub>CO and CH<sub>3</sub>OH (see Figure 4 in Paper I). In line with our results exploratory chemical models from Dzyurkevich et al. (2020) show that SO is the primary S-carrier in the gas phase in a IRS 48 like disk model. They also show that the SO<sub>2</sub> abundance is sensitive to the dust-to-gas mass ratio in the disk, therefore the SO/SO<sub>2</sub> ratio may be a useful complementary tracer of the gas and dust properties of vortices.

A particular disk to compare to IRS 48 is AB Aur as they both host azimuthal dust traps. In AB Aur SO has been detected and shows a ring-like morphology (Rivière-Marichalar et al. 2020). SO emission over the full azimuth could be explained by AB Aur hosting a less azimuthally concentrated dust trap than in IRS 48 as the millimeter grains are detected throughout the whole azimuth of the AB Aur disk (see Figure 2 in van der Marel et al. 2021, note this is not Paper I, for a comparison of the mm-dust emission from both disks). Therefore, this is still consistent with our proposed scenario for the IRS 48 disk hosting a particularly massive ice trap with a low gas to dust ratio at the trap.

We derive a SO/SO<sub>2</sub> ratio of 1.5-1.8 (see Table 2) which is closest with the values found for Hale-Bopp (SO/SO<sub>2</sub>=1.3; Bockelée-Morvan et al. 2000) and the Class I disk Elias 29 (SO/SO<sub>2</sub>=2.0; Oya et al. 2019). These values are a factor of a few higher than measured in IRAS 16293-2422 B (SO/SO<sub>2</sub>=0.3) and the comet 67P (SO/SO<sub>2</sub>=0.4-0.7) (Calmonte et al. 2016; Drozdovskaya et al. 2018). The chemistry in the disk is not solely due to thermal desorption but is also driven by the UV and X-ray irradiation fields. This would result in the photo-dissociation of SO<sub>2</sub> to form SO accounting for the higher SO/SO<sub>2</sub> ratio we observe towards IRS 48 than IRAS 16293-2422 B. In photo-dissociation regions this value is indeed higher with, e.g. SO/SO<sub>2</sub>≈10 in the Horsehead Nebula (Rivière-Marichalar et al. 2019) and ≈3 in the extended ridge of the Orion Bar compared with 0.4 at the location of the hot core (Crockett et al. 2014).

#### 4.3. Constraints on the C/O ratio of the gas

The non-detection of CS in a disk that is rich in emission from volatile sulphur molecules may appear puzzling. Our 3 $\sigma$  upper-limit on the CS column density is at the high end of the values detected in other sources which cover more than one order of magnitude ( $\times 10^{12} - 10^{13} \text{ cm}^{-2}$ ) (Semenov et al. 2018; Le Gal et al. 2019). In these other disks the inferred CS/SO ratios are >1000 $\times$  higher than our observations (CS/SO < 0.01) and the detection of CS and the non-detection of SO (and SO<sub>2</sub>) have

been used to infer the C/O ratio in the warm molecular layer. Chemical modelling shows that the CS/SO abundance ratio is the most sensitive to the overall C/O ratio in the gas rather than other physical/chemical processes, e.g., grain growth, UV irradiation and turbulent mixing (Semenov et al. 2018; Fedele & Favre 2020). Disk specific modelling efforts show that CS/SO ratios of order 100 can be re-produced via gas-phase chemistry where the C/O ratio is super-solar (>1) (Dutrey et al. 2011; Semenov et al. 2018). Even in AB Aur, where SO is detected, an elevated C/O ratio of 1.0 is favoured in the chemical modelling (Rivière-Marichalar et al. 2020). Recent observations of the transition disk PDS 70 also report a CS/SO >100 which is in line with a C/O>1 (Facchini et al. 2021). This means that the bulk of gas accreted by forming planets in these disks is oxygen poor.

In the IRS 48 disk we have the opposite situation where the CS/SO <0.01 (see Table 2). From a comparison to chemical models our column density ratios suggest a solar C/O ratio (Semenov et al. 2018). A complementary test of high C/O ratio in IRS 48 would be the detection/non-detection of strong C<sub>2</sub>H emission (e.g. Bergin et al. 2016) and other oxygen rich molecules like H<sub>2</sub>O. In general, the sublimation of ices at the edge of the cavity means that the gas accreted through the cavity onto potential forming planets will have significantly different elemental composition to the gas accreted by a planet forming in a gap further out in a disk. This is in contrast to what has been proposed for TW Hya (Bosman & Banzatti 2019) where the dust trap is beyond the CO ice line and thus the inner disk gas is volatile poor.

Another transition disk with an azimuthal asymmetry is HD 142527. CS has been detected in this disk and is also asymmetric but it is anti-coincident with the dust trap peaking on the other side of the disk (van der Plas et al. 2014). The authors propose that this is either due to the lower temperatures in the dust trap resulting in the freeze-out of molecules or the high optical depth of the dust obstructing the line emission from the dust trap region. But, it could alternatively be tracing an azimuthal change in the C/O ratio where C/O <1 in the region of the dust trap due to the sublimation of ices.

## 5. Conclusions

In this letter we have presented ALMA observations targeting the S-bearing molecules SO, SO<sub>2</sub> and CS in the unique Oph-IRS 48 disk hosting a massive ice trap. We summarise our conclusions here:

- This is the first robust detection of SO<sub>2</sub> and the isotopologue <sup>34</sup>SO<sub>2</sub> in a Class II disk.
- These oxygen rich S-bearing molecules have a clear disk origin unlike in other sources where they trace shocks or winds/outflows.
- As the sulphur species are co-spatial with the dust trap we suggest that presence of the gas-phase SO and SO<sub>2</sub> is due to the sublimation of ices at the edge of the dust cavity and that the bulk of the ice reservoir is coincident with the millimeter, and larger, dust grains.
- We estimate the average S/H from the SO and SO<sub>2</sub> column densities to be  $4.6 - 10.0 \times 10^{-7}$  and this is consistent with 15-100 % of the total expected volatile sulphur budget in the disk.
- Unlike all other protoplanetary disks targeted in these molecules so far, CS is not the primary S-carrier in the gas phase and the CS/SO ratio is <0.01 in strong contrast to other disks.

- The inferred gas-phase C/O ratio  $<1$  and is likely solar. We propose that this is due to the chemistry being driven by the sublimation of ices rather than gas-phase processes. This is a result of the unique nature of the extreme dust trap in the IRS 48 disk. This has important implications for the elemental composition of the atmosphere of gas-giant planets that maybe be forming or will form in this disk.

This work and Paper I further showcases the use of transition disks as unique observational laboratories to explore the full volatile inventory in disks due to the sublimation of ices at the cavity edge.

## References

- Artur de la Villarmois, E., Jørgensen, J. K., Kristensen, L. E., et al. 2019, A&A, 626, A71
- Bergin, E. A., Du, F., Cleeves, L. I., et al. 2016, ApJ, 831, 101
- Bockelée-Morvan, D., Lis, D. C., Wink, J. E., et al. 2000, A&A, 353, 1101
- Boogert, A. C. A., Gerakines, P. A., & Whittet, D. C. B. 2015, ARA&A, 53, 541
- Boogert, A. C. A., Schutte, W. A., Helmich, F. P., Tielens, A. G. G. M., & Wooden, D. H. 1997, A&A, 317, 929
- Booth, A. S., Walsh, C., Kama, M., et al. 2018, A&A, 611, A16
- Booth, A. S., Walsh, C., Terwisscha van Scheltinga, et al. 2021, Nature Astronomy (subm)
- Booth, R. A., Clarke, C. J., Madhusudhan, N., & Ilee, J. D. 2017, MNRAS, 469, 3994
- Bosman, A. D. & Banzatti, A. 2019, A&A, 632, L10
- Brown, J. M., Herczeg, G. J., Pontoppidan, K. M., & van Dishoeck, E. F. 2012, ApJ, 744, 116
- Bruderer, S., van der Marel, N., van Dishoeck, E. F., & van Kempen, T. A. 2014, A&A, 562, A26
- Calmonte, U., Altwegg, K., Balsiger, H., et al. 2016, MNRAS, 462, S253
- Carney, M. T., Hogerheijde, M. R., Guzmán, V. V., et al. 2019, A&A, 623, A124
- Charnley, S. B. 1997, ApJ, 481, 396
- Cleeves, L. I., Bergin, E. A., Bethell, T. J., et al. 2011, ApJ, 743, L2
- Codella, C., Podio, L., Garufi, A., et al. 2020, arXiv e-prints, arXiv:2011.02305
- Cridland, A. J., Bosman, A. D., & van Dishoeck, E. F. 2020, A&A, 635, A68
- Crockett, N. R., Bergin, E. A., Neill, J. L., et al. 2014, ApJ, 787, 112
- Drozdovskaya, M. N., van Dishoeck, E. F., Jørgensen, J. K., et al. 2018, MNRAS, 476, 4949
- Dutrey, A., Guilloteau, S., & Guelin, M. 1997, A&A, 317, L55
- Dutrey, A., Wakelam, V., Boehler, Y., et al. 2011, A&A, 535, A104
- Dzyurkevich, N., Lyra, W., & Majumdar, L. 2020, in Origins: From the Protosun to the First Steps of Life, ed. B. G. Elmegreen, L. V. Tóth, & M. Güdel, Vol. 345, 285–286
- Eistrup, C., Walsh, C., & van Dishoeck, E. F. 2018, A&A, 613, A14
- Facchini, S., Teague, R., Bae, J., et al. 2021, arXiv e-prints, arXiv:2101.08369
- Fedele, D., Bruderer, S., van Dishoeck, E. F., et al. 2013, A&A, 559, A77
- Fedele, D. & Favre, C. 2020, A&A, 638, A110
- Francis, L. & van der Marel, N. 2020, ApJ, 892, 111
- Fuente, A., Cernicharo, J., Agúndez, M., et al. 2010, A&A, 524, A19
- Gaia Collaboration, Brown, A. G. A., Vallenari, A., et al. 2018, A&A, 616, A1
- Garufi, A., Podio, L., Codella, C., et al. 2021, A&A, 645, A145
- Geers, V. C., Pontoppidan, K. M., van Dishoeck, E. F., et al. 2007, A&A, 469, L35
- Goldsmith, P. F. & Langer, W. D. 1999, ApJ, 517, 209
- Guilloteau, S., Reboussin, L., Dutrey, A., et al. 2016, A&A, 592, A124
- He, C., Hörst, S. M., Lewis, N. K., et al. 2020, Nature Astronomy, 4, 986
- Jenkins, E. B. 2009, ApJ, 700, 1299
- Kama, M., Shorttle, O., Jermyn, A. S., et al. 2019, ApJ, 885, 114
- Keller, L. P., Hony, S., Bradley, J. P., et al. 2002, Nature, 417, 148
- Krijt, S., Bosman, A. D., Zhang, K., et al. 2020, ApJ, 899, 134
- Le Gal, R., Öberg, K. I., Huang, J., et al. 2020, ApJ, 898, 131
- Le Gal, R., Öberg, K. I., Loomis, R. A., Pegues, J., & Bergner, J. B. 2019, ApJ, 876, 72
- Loomis, R. A., Cleeves, L. I., Öberg, K. I., et al. 2018, ApJ, 859, 131
- Meheut, H., Casse, F., Varniere, P., & Tagger, M. 2010, A&A, 516, A31
- Morbidelli, A., Szulágyi, J., Crida, A., et al. 2014, Icarus, 232, 266
- Müller, H. S. P., Schlöder, F., Stutzki, J., & Winnewisser, G. 2005, Journal of Molecular Structure, 742, 215
- Ohashi, S., Kataoka, A., van der Marel, N., et al. 2020, ApJ, 900, 81
- Oya, Y., López-Sepulcre, A., Sakai, N., et al. 2019, ApJ, 881, 112
- Phuong, N. T., Chapillon, E., Majumdar, L., et al. 2018, A&A, 616, L5
- Ranjan, S., Todd, Z. R., Sutherland, J. D., & Sasselov, D. D. 2018, Astrobiology, 18, 1023
- Rivière-Marichalar, P., Fuente, A., Goicoechea, J. R., et al. 2019, A&A, 628, A16
- Rivière-Marichalar, P., Fuente, A., Le Gal, R., et al. 2020, A&A, 642, A32
- Salinas, V. N., Hogerheijde, M. R., Bergin, E. A., et al. 2016, A&A, 591, A122
- Semenov, D., Favre, C., Fedele, D., et al. 2018, A&A, 617, A28
- Teague, R., Bae, J., & Bergin, E. A. 2019, Nature, 574, 378
- Tieftunk, A., Pineau des Forets, G., Schilke, P., & Walmsley, C. M. 1994, A&A, 289, 579
- Tychoniec, L., van Dishoeck, E. F., van 't Hoff, M. L. R., & et al. 2021, submitted A&A
- van der Marel, N., Birnstiel, T., Garufi, A., et al. 2021, AJ, 161, 33
- van der Marel, N. & et al. 2021, AJ
- van der Marel, N., Pinilla, P., Tobin, J., et al. 2015, ApJ, 810, L7
- van der Marel, N., van Dishoeck, E. F., Bruderer, S., et al. 2016, A&A, 585, A58
- van der Marel, N., van Dishoeck, E. F., Bruderer, S., et al. 2013, Science, 340, 1199
- van der Marel, N., van Dishoeck, E. F., Bruderer, S., & van Kempen, T. A. 2014, A&A, 563, A113
- van der Plas, G., Casassus, S., Ménard, F., et al. 2014, ApJ, 792, L25
- Walsh, C., Loomis, R. A., Öberg, K. I., et al. 2016, ApJ, 823, L10
- Wilson, T. L. 1999, Reports on Progress in Physics, 62, 143
- Woods, P. M., Occhiogrosso, A., Viti, S., et al. 2015, MNRAS, 450, 1256
- Öberg, K. I., Murray-Clay, R., & Bergin, E. A. 2011, The Astrophysical Journal, 743, L16

*Acknowledgements.* We would like to thank Akimasa Kataoka for his help with the reduction of the data. N.M. acknowledges support from the Banting Postdoctoral Fellowships program, administered by the Government of Canada. ALMA is a partnership of ESO (representing its member states), NSF (USA) and NINS (Japan), together with NRC (Canada) and NSC and ASIAA (Taiwan) and KASI (Republic of Korea), in cooperation with the Republic of Chile. The Joint ALMA Observatory is operated by ESO, AUI/ NRAO and NAOJ. This paper makes use of the following ALMA data: 2013.1.00100.S, 2017.1.00834.S.

## Appendix A: Additional Figures

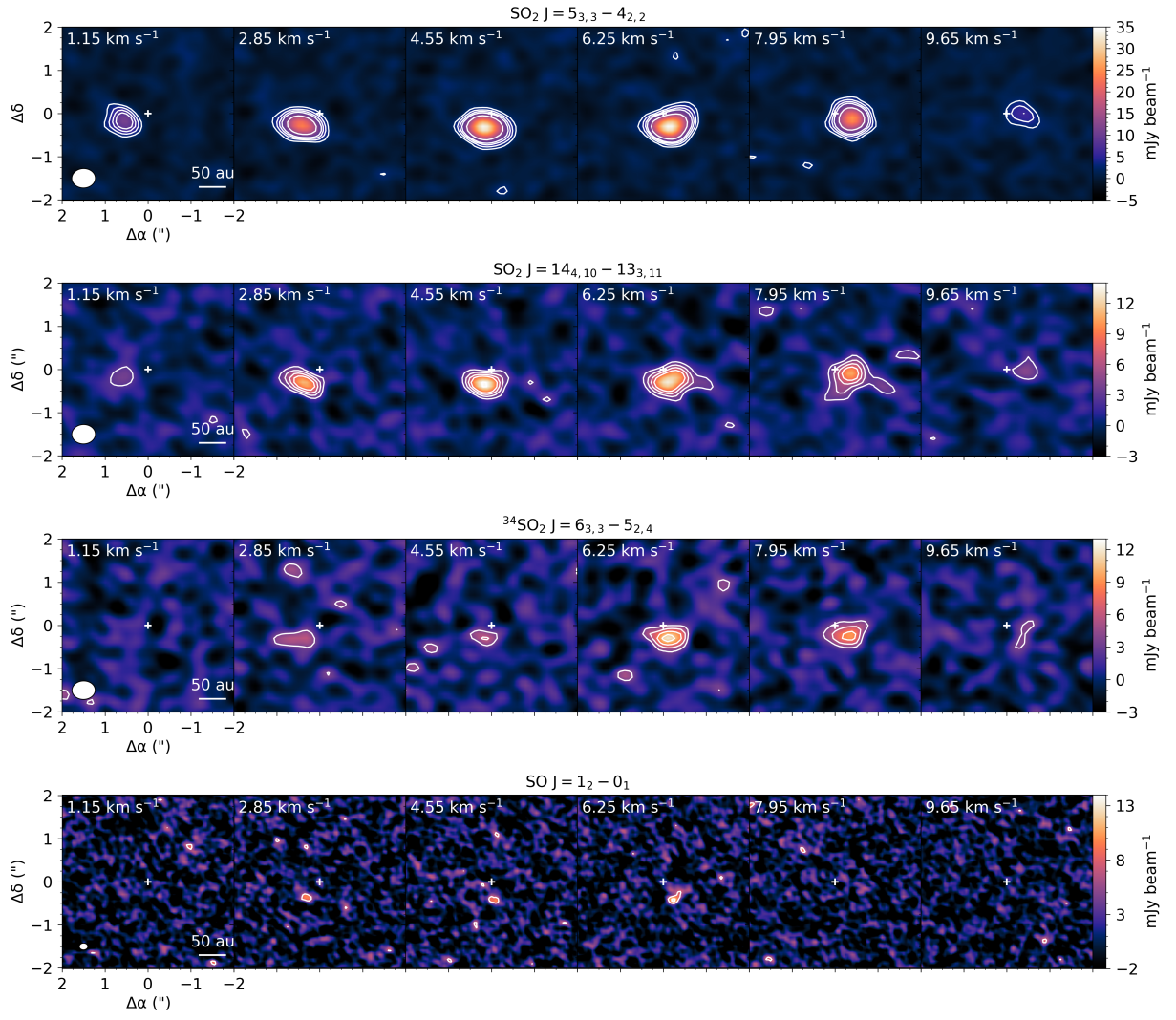


**Fig. A.1.** Channel maps of the detected SO, SO<sub>2</sub> and <sup>34</sup>SO<sub>2</sub> where the contours mark  $[3, 5, 7, 9, 15] \times \sigma$  where  $\sigma$  is the rms listed in Table 1.



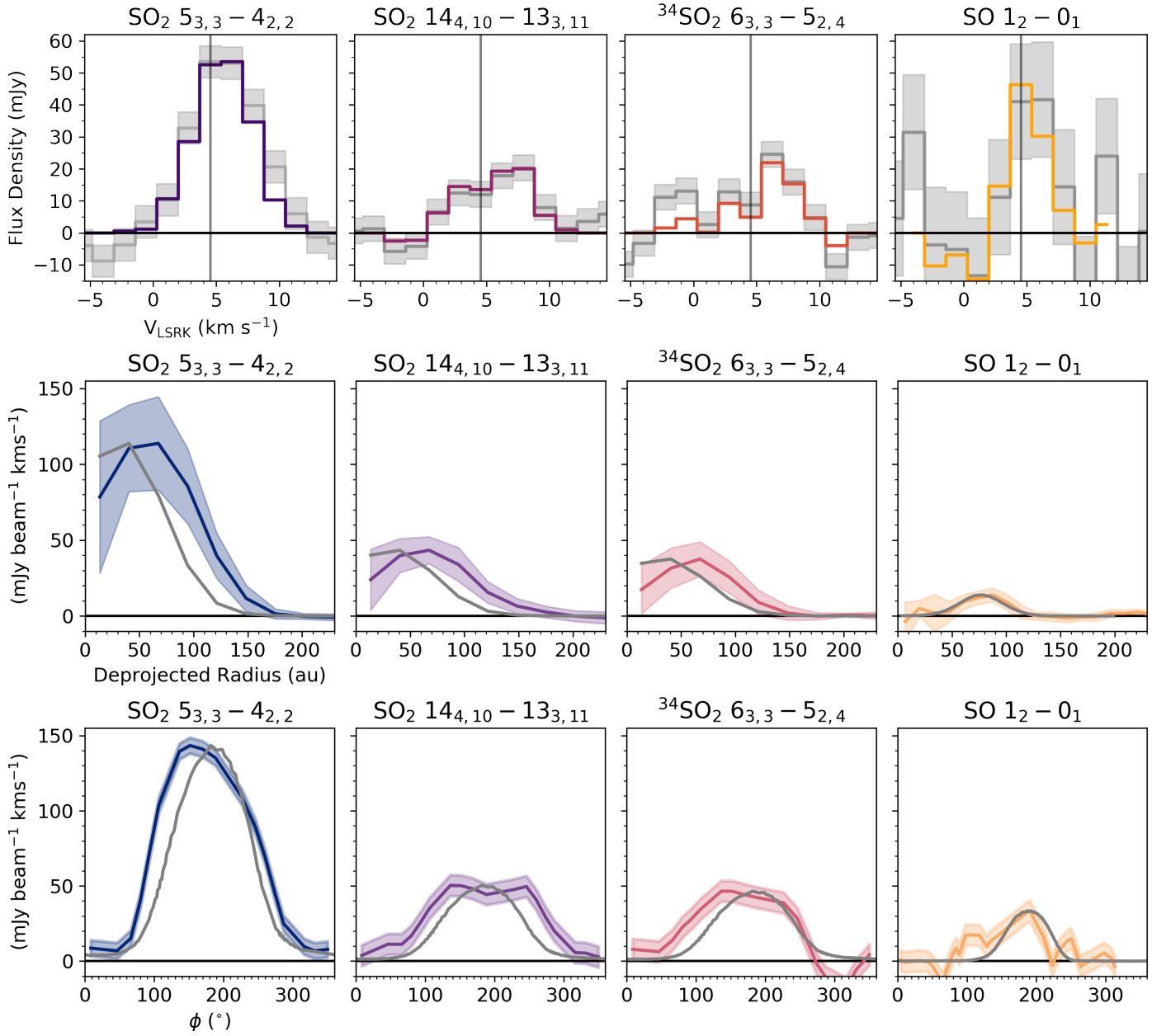


**Fig. A.2.** Top: Spectra extracted from Keplerian masks (colours) and 1''5 ellipse centred on source (grey) with  $\pm 1\sigma$  error bars. Grey line marks the source velocity ( $4.55 \text{ km s}^{-1}$ ). Middle: Radial emission profiles averaged over wedge from  $100^\circ$  to  $260^\circ$ . Grey profiles are the dust emission at the same resolution as the line data and error bars on the line profiles are shaded regions. Bottom: Azimuthal profiles extracted at a deprojected radius of 70 au for the SO<sub>2</sub> lines and 90 au for the SO lines. The grey lines show the dust azimuthal profile extracted at the same radius for each line respectively.

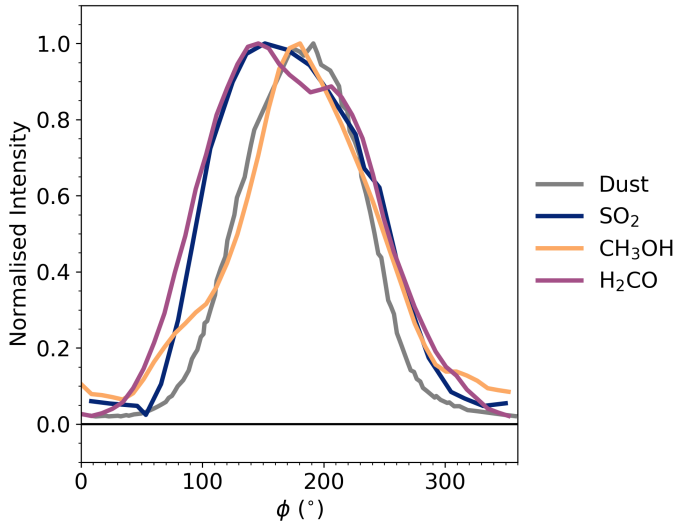


**Fig. A.3.** Normalised azimuthal profiles of 0.9 mm dust,  $\text{H}_2\text{CO}$  (transition),  $\text{CH}_3\text{OH}$  (transition) and  $\text{SO}_2$  ( $J = 5_{3,3} - 4_{2,2}$ ) lines taken at 70 au. The  $\text{H}_2\text{CO}$  and  $\text{CH}_3\text{OH}$  data are from van der Marel & et al. (2021).

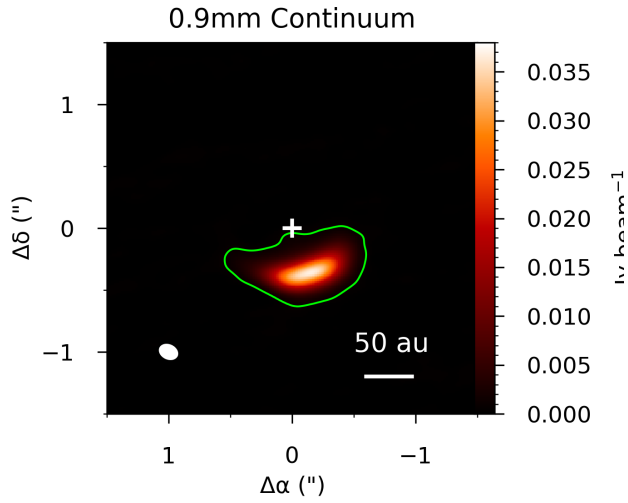


**Fig. A.4.** 0.9 mm continuum emission from Francis & van der Marel (2020). Green contour is the  $5\sigma$  level and is the area used to calculate the column densities.